



HAL
open science

Two Propagation Scenarios of Isolated Breakdown Lightning Processes in Failed Negative Cloud-to-Ground Flashes

Ivana Kolmašová, Ondřej Santolík, Eric Defer, Petr Kašpar, Andrea Kolínská,
Stéphane Pedeboy, Sylvain Coquillat

► **To cite this version:**

Ivana Kolmašová, Ondřej Santolík, Eric Defer, Petr Kašpar, Andrea Kolínská, et al.. Two Propagation Scenarios of Isolated Breakdown Lightning Processes in Failed Negative Cloud-to-Ground Flashes. Geophysical Research Letters, 2020, 47 (23), 10.1029/2020GL090593 . hal-03042155

HAL Id: hal-03042155

<https://hal.science/hal-03042155>

Submitted on 8 Dec 2020

HAL is a multi-disciplinary open access archive for the deposit and dissemination of scientific research documents, whether they are published or not. The documents may come from teaching and research institutions in France or abroad, or from public or private research centers.

L'archive ouverte pluridisciplinaire **HAL**, est destinée au dépôt et à la diffusion de documents scientifiques de niveau recherche, publiés ou non, émanant des établissements d'enseignement et de recherche français ou étrangers, des laboratoires publics ou privés.

1 **Two propagation scenarios of isolated breakdown lightning processes in failed negative**
2 **cloud-to-ground flashes**

3

4 Ivana Kolmašová

5 Department of Space Physics, Institute of Atmospheric Physics of the Czech Academy of
6 Sciences, Prague, Czechia

7 Faculty of Mathematics and Physics, Charles University, Prague, Czechia

8

9 Ondřej Santolík

10 Department of Space Physics, Institute of Atmospheric Physics of the Czech Academy of
11 Sciences, Prague, Czechia

12 Faculty of Mathematics and Physics, Charles University, Prague, Czechia

13

14 Eric Defer

15 Laboratoire d'Aérodynamique, Université de Toulouse, CNRS, OMP, UPS, Toulouse, France

16

17 Petr Kašpar

18 Department of Space Physics, Institute of Atmospheric Physics of the Czech Academy of
19 Sciences, Prague, Czechia

20

21 Andrea Kolínská

22 Department of Space Physics, Institute of Atmospheric Physics of the Czech Academy of
23 Sciences, Prague, Czechia

24 Faculty of Nuclear Sciences and Physical Engineering, Czech Technical University, Prague,
25 Czechia

26

27 Stéphane Pedeboy

28 Météorage, Pau, France

29

30 Sylvain Coquillat

31 Laboratoire d'Aérodynamique, Université de Toulouse, CNRS, OMP, UPS, Toulouse, France

32

33

34 Corresponding author: I. Kolmašová, Institute of Atmospheric Physics of the Czech Academy of
35 Sciences, Boční II 1401, 141 00 Prague 4, Czechia (iko@ufa.cas.cz)

36

37 **Key points**

- 38 • Preliminary breakdown radiowave pulses typical for negative cloud-to-ground flashes are
39 exceptionally observed without return strokes.
- 40 • Data show evidence of two possible propagation scenarios: the discharge leader either
41 extends horizontally inside the cloud or fades out.
- 42 • The first analysis of a large number of events shows that waveform characteristics of pulse
43 trains are very similar for both scenarios.

44

45 **Plain language summary**

46

47 Visible lightning return stroke represents a well-known manifestation of atmospheric electricity.
48 However, it is only the last stage of a complex sequence of phenomena that starts inside an
49 electrically charged thundercloud by a preliminary breakdown process, continues by a stepped
50 leader that moves electrical charges into the lightning channel, neutralized eventually by a large
51 return stroke current and followed in most cases by processes leading to subsequent strokes. All
52 these phenomena occurring inside or below the thundercloud involve impulsive electrical currents
53 and hence emit radio waves. Analysis of our observations of isolated breakdown radiowave pulses,
54 which are not followed by a return stroke shows that the underlying processes are similar to a usual
55 preliminary breakdown preceding negative cloud-to ground discharges. Nevertheless, a strong
56 positive charge layer at the bottom of the thundercloud can force the breakdown current pulses to
57 keep flowing inside the cloud or die out, and thus prevents them from evolving into a return stroke
58 that would move the negative charge from the cloud to the ground.

59

60 **Abstract**

61 Isolated breakdown process (also known as attempted leader or inverted intra-cloud discharge) is
62 a lightning phenomenon characterized by radiowave pulses similar to signatures of preliminary
63 breakdown before negative cloud-to-ground flashes, but in this case no cloud-to-ground return
64 strokes occur. We identified 128 isolated breakdown pulse trains in measurements collected in the
65 Mediterranean by a broadband receiver (0.005 – 37 MHz) in 2015 and 2018. By combining these
66 records with concurrent Lightning Mapping Array measurements of very high frequency radiation
67 (60 – 66 MHz) emitted by in-cloud discharges we investigate the development of each discharge.
68 We identify two scenarios: either the discharges continue to propagate almost horizontally for
69 more than 150 ms (73%), or they quickly fade out (27%). The geo-localized sources of the
70 observed isolated breakdown pulse trains, together with their waveform characteristics (duration,
71 inter-pulse intervals, regularity, bipolar shapes) show that both scenarios are similar to initiation
72 processes preceding negative cloud-to-ground flashes.

73

74

75

76 **Index terms:** 3304 Atmospheric electricity

77 3324 Lightning

78 3394 Instruments and techniques

79

80

81 **1. Introduction**

82 Both cloud-to-ground (CG) and intra-cloud (IC) lightning flashes usually start with a
83 preliminary breakdown (PB) process (sometimes referred to as initial breakdown) which is
84 characterized by a presence of trains of bipolar pulses in electromagnetic recordings (Marshall et
85 al., 2014a and references herein). These pulse trains are emitted by in-cloud currents and can be
86 detected hundreds of kilometers from their source (Kolmasova et al., 2016, Kotovsky et al.,
87 2016). Measurements conducted several kilometers from lightning recently showed that the first
88 PB pulse is preceded by an ionizing initiation event followed by an initial electric field change
89 (Marshall et al., 2014b, 2019). The PB stage of negative CG lightning flashes usually converts
90 into a stepped leader followed by the first return stroke (RS) (Rakov & Uman, 2003 and
91 references herein).

92 However, sometimes the pre-stroke activity does not lead to a regular RS pulse. Norinder
93 and Knudsen (1956) reported for the first time an observation of “pre-discharges lacking the
94 main discharge”. Nag and Rakov (2008) described observation of trains of electric field pulses,
95 which were not followed by RS pulses. These isolated trains possessed characteristics of PB
96 sequences preceding negative CG discharges. They named them “first attempted cloud-to-ground
97 leaders”. Sharma et al. (2008) introduced a term “isolated breakdown” for PB sequences which
98 did not lead to any subsequent activity and compared properties of isolated breakdown pulse
99 trains with those leading to RSs They found that durations of pulse trains and inter-pulse time
100 intervals were comparable for isolated breakdown and PB pulse trains. Kolmasova et al. (2018)
101 showed that an intense radiation in a frequency band 60-66 MHz abruptly started with the first
102 pulse and was present during the entire pulse train of both regular PB and isolated breakdown
103 processes. Ma (2017) used the term PB-type flashes for PB pulses not followed by negative CG
104 and found them to occur at the early stage of isolated thunderstorms. Zhang et al. (2002) reported

105 the polarity-inverted IC discharges, which originated from the middle negative charge region and
106 propagated downward to the lower positive charge region (LPCR), where they developed
107 horizontally. Qie et al. (2008) found a majority of IC discharges to originate in the lower dipole
108 during a major stage of a hailstorm at Tibetan Plateau. They called them lower level IC flashes
109 and speculated that hails in the lower part of the cloud substantially contribute to the unusual
110 strength of the LPCR. Zhang et al. (2015) hypothesized that the initiation processes of the
111 inverted IC discharges, normal negative CG discharges and hybrid IC-CG discharges did not
112 differ and that their later differentiation was controlled by the strength of the LPCR. Chilingarian
113 et al. (2020) observed a termination of terrestrial gamma-ray enhancements by inverted IC
114 discharges. This means that electric field between the main negative charge region and the LCPR
115 was strong enough to accelerate electrons.

116 The role of LPCR in an evolution of discharges was also intensively modeled (Nag and
117 Rakov, 2009; Tan et al., 2005; Iudin et al., 2017). Tan et al. (2014) found that the types and
118 polarities of lightning discharges might depend on locations and magnitudes of oppositely
119 charged layers near initiation points. For negative CG flashes, the magnitude of the LPCR near
120 the lightning initiation needed to be strong enough for initiation breakdown, however an
121 exceptionally strong LPCR could obstruct further propagation of the discharge down to the
122 ground. Iudin et al. (2017) similarly concluded that a strong LPCR could block further vertical
123 extension of the discharge.

124 This overview shows that lightning events characterized by PB pulses, which fail to
125 evolve into negative stepped leaders and subsequent return strokes, were given different labels in
126 the literature: “attempted CG leaders” (Nag and Rakov, 2008,2009), “isolated breakdown ”
127 (Sharma et al, 2008; Esa et al., 2013a,b; Kolmasova et al., 2018), “inverted IC discharges”

128 (Zhang et al., 2002, 2015; Nag and Rakov, (2009); Chilingarian et al., 2020), “low-level IC
129 flashes” (Qie et al., 2008), or “PB-type flashes” (Ma, 2017). All these expressions probably
130 describe the same phenomenon. Out of these possibilities, we think that “isolated breakdown” is
131 the best term to characterize what actually happens in the cloud, because properties of these
132 events are far from normal IC discharges, but close to the breakdown processes preceding
133 normal negative CG discharges.

134 In the present letter, we report results of our new investigation of properties of the
135 isolated breakdown processes including their pulse train characteristics and propagation
136 schemes. Our analysis is based on a combination of broadband magnetic-field measurements,
137 narrowband electric-field Lightning Mapping Array (LMA) records, and Low Frequency
138 detections of the French operational Météorage network. For the first time, we discuss this
139 phenomenon based on larger number of cases compared to previous studies dealing only with
140 several cases (Zhang et al. 2002; Coleman et al. 2008). Our analysis of more than 100 isolated
141 breakdown events allows us to draw new conclusions about their propagation schemes. The
142 observations were collected in Mediterranean during two observational campaigns in September
143 - November 2015 and September - November 2018 in the frame of the SOLID (Space-based
144 Optical Lightning Detection) and the EXAEDRE (EXploiting new Atmospheric Electricity Data
145 for Research and the Environment) projects, respectively. Our results show that the duration of
146 isolated breakdown pulse trains, the inter-pulse intervals, and the regularity of their temporal
147 distribution in the analyzed events are similar to PB processes preceding regular CG discharges
148 but are very different from typical initial breakdown processes of normal IC discharges. We
149 present for the first time two typical scenarios of the isolated breakdown processes: (i) negative
150 leaders keep propagating horizontally for more than 150 ms (73%) or (ii) discharges

151 substantially weaken within the same time interval (27%). In sections 2 and 3 we describe both
152 instrumental setup and dataset. In section 4, we present results of our analysis of the
153 measurements. In section 6, we discuss and summarize our results.

154

155 **2. Instrumentation**

156 To detect fluctuations of the E-W horizontal component of magnetic field we use the
157 broadband analyzer BLESKA (Broadband Lightning Electromagnetic Signal Keeper Analyzer)
158 (Kolmasova et al., 2018), a clone of the IME-HF analyzer (Instrument de Mesure du champ
159 Electrique Haute Fréquence) developed for the TARANIS (Tool for the Analysis of Radiation
160 from lightning and Sprites) spacecraft (Blanc et al., 2007) and adapted for ground-based
161 measurements. The analyzer is connected to the magnetic sensor SLAVIA (Shielded Loop
162 Antenna with a Versatile Integrated Amplifier) and detects signals in the frequency range from 5
163 kHz to 37 MHz, sampled at 80 MHz. The absolute time is obtained from a GPS receiver with an
164 accuracy of 1 μ s. The duration of triggered waveform snapshots is 208 ms. The receiver was
165 installed close to Ersa, France (550 m, 42.97°N, 9.38°E), at the northernmost point of the Corsica
166 island, in 2015. It was moved by a few kilometers in 2018 (100 m, 43.00°N, 9.36°E). BLESKA
167 detects broadband pulses exhibiting peak-to-peak amplitudes larger than 0.4 nT which is well
168 above the level of environmental interferences.

169 The magnetic field records are combined with the measurements of 12-LMA-station
170 SAETTA (Suivi de l'Activité Electrique Tridimensionnelle Totale de l'Atmosphère) network
171 operated in Corsica since June 2014 (Rison et al., 1999; Coquillat et al., 2019). Each station is
172 equipped with an electric-field antenna and detects very high frequency (VHF) radiation emitted
173 by lightning discharges in the 60-66 MHz band and sampled at 25 MHz. In each 80- μ s time
174 interval, the individual stations identify the times of arrival of the strongest VHF peak exceeding

175 a predefined threshold. The arrival times of the radiation peaks coming from the same source and
176 detected by at least six individual LMA stations are used to calculate the 3D-location of a VHF
177 radiation source. SAETTA also estimates power of individual geo-located VHF sources. GPS
178 receivers are connected to each LMA station and provide a time assignment with an accuracy of
179 $1 \mu\text{s}$ (Thomas et al., 2004).

180 Locations, polarities, and peak currents for discharges used in our study were provided by
181 the French lightning locating system Météorage. To achieve an optimum coverage of the South-
182 East France and Corsica regions it combines sensors installed across France, and sensors
183 operated by Italian national service SIRF. The detection efficiency is 94%, the median location
184 accuracy 120 meters (Pedeboy and Toullec, 2016) and the accuracy of estimation of peak current
185 amplitudes is about 18% (Schulz et al., 2016). Characteristics of both CG and IC discharges were
186 available for both 2015 and 2018 datasets with an improved IC discharge detection efficiency for
187 2018.

188

189 **3. Dataset**

190 We visually inspected all triggered 208-ms long magnetic-field waveform captures recorded
191 by BLESKA during autumn 2015 and autumn 2018 in order to identify sequences of bipolar
192 pulses. We have chosen only the magnetic-field records containing pulse trains during which
193 SAETTA was able to geo-locate at least one VHF source. To distinguish isolated breakdown
194 events from usual PB pulses preceding -CG lightning and from PB preceding normal IC
195 discharges, we used the following criteria:

- 196 i) RS pulses were absent after the initial pulse sequence within the 208-ms long magnetic-
197 field waveform snapshots.

198 ii) The list of Météorage records did not contain any CG detection within 1s after the time of
199 the strongest isolated breakdown pulse in magnetic field records.

200 iii) Knowing that the usual PB pulses have the same initial polarity as the corresponding RS
201 pulses (Rakov and Uman, 2003), we selected only trains of pulses that exhibited the same
202 polarity as negative RS pulses. This criterion together with a visual inspection of the pulse
203 train waveforms leads to the exclusion of PB pulse trains preceding normal polarity IC
204 discharges. We were able to check the pulse polarity without any ambiguity by combining
205 the magnetic loop antenna orientation with the locations of the IC pulses detected by
206 Météorage. By applying this polarity criterion, we reduced our dataset by 20 %. We verified
207 that the arrival azimuth of all analyzed events was further than 2 degrees from the eastward
208 and westward directions (perpendicular to our magnetic loop) to avoid any misclassification
209 of the polarity. A visual inspection of excluded trains showed that all excluded events
210 lacked at least one typical signature of PB pulse trains preceding -CGs: i.e., duration of
211 about 1-2 ms, inter-pulse intervals of about 100 μ s, and a regular temporal distribution of
212 pulses (Nag and Rakov, 2008). We also noted that the peak amplitude of pulses randomly
213 varied within the trains for all excluded events.

214 The resulting dataset consists of 128 isolated breakdown events (33 events in 2015; 95
215 events in 2018).

216

217 **4. Data Analysis**

218 The sequences of the isolated breakdown pulses identified in the magnetic-field records
219 were usually a few milliseconds long. They were preceded by an electromagnetically quiet
220 period lasting several tens of milliseconds in all cases. The inter-pulse intervals lasted from
221 several tens of microseconds to a few hundred of microseconds. The strongest pulses in

222 individual sequences usually occur during the first millisecond after the first recognizable pulse.
223 The pulse activity following the sequences of the isolated breakdown pulses was weak or
224 completely absent. Two examples of magnetic-field waveforms containing the isolated
225 breakdown events recorded by BLESKA are shown in Figs. 1a and 2a, displaying a detail of 3
226 ms, while Figs. 1b, 1c, 2b, and 2c present the whole 208-ms long waveforms. Waveforms in Fig.
227 1 and Fig. 2 were respectively captured on October 2, 2018 and October 13, 2015. Red arrows
228 point at the time of Météorage IC detections. Their peak currents were estimated to 16.2 kA and
229 9.4 kA, respectively.

230 Correspondence of the isolated breakdown pulses measured by BLESKA and the VHF
231 sources geo-located by SAETTA is shown in Fig. 1a, 1b, 2a, and 2b: each dot corresponds to one
232 reconstructed source of VHF radiation color-coded by its power. It is evident from Figs. 1a and
233 2a that almost none of the observed isolated breakdown pulses have a counterpart within the geo-
234 located VHF radiation sources during the displayed three milliseconds. This effect was already
235 reported by Kolmasova et al., 2018, and explained by a decreased ability of the LMA system to
236 geo-locate VHF sources if the counts of samples above the threshold reached a maximum of
237 2000 (40-ns) detections within an 80- μ s LMA window at individual stations. This maximum of
238 2000 detections was regularly reached at the LMA stations located close to developing
239 discharges suggesting that continuous VHF radiation was received during the initial phase of the
240 isolated breakdown events. During the 208 ms-long records in Figs. 1b and 2b, SAETTA was
241 able to geo-locate 444 and 159 VHF sources, respectively. The number of geo-locations during
242 all 128 events varies from 1 (our condition for including an event in the analysis) to 843 VHF
243 sources. The first geo-located VHF source occurred within the ± 1 ms window around the first
244 detectable isolated breakdown pulse in 75 % of cases. In more than 85 % of events, the geo-

245 located VHF source occurring close to the first detectable magnetic-field pulse was also the most
246 powerful one, with power varying from 8 to 36 dBW (24 dBW on average). Geo-located VHF
247 sources occurring later in time were weaker in amplitude, and, similarly as in Figs. 1b and 2b,
248 their power did not exceed 20 dBW. VHF sources were predominantly reconstructed at an
249 altitude between 2 and 6 km, even if some sources appeared also below and above this altitude
250 range (for an overview, see animations S1 and S2 in the Supporting Information). We also noted
251 localized VHF sources, which did not have their counterparts in the broadband waveforms.
252 These VHF sources occurred especially in the later part of the records, well behind the train of
253 the isolated breakdown pulses. This effect can be explained by a lower sensitivity of the
254 broadband analyzer to signals generated by horizontal currents. We also speculate that during the
255 horizontal propagation of the discharges, the in-cloud channels might become shorter, and as a
256 result, the frequency of emitted radiation might have shifted above the upper frequency limit of
257 the broadband receiver (37 MHz) but still stay detectable by SAETTA at 66 MHz. Kolmasova et
258 al. (2018) reported that individual peaks of strong VHF radiation recorded at individual stations
259 (raw LMA data) still corresponded well to the broadband pulses during lightning initiation, even
260 in the situation when the LMA was unable to reconstruct geo-located VHF sources. Examples of
261 VHF radiation detected by SAETTA station B are illustrated in Figs. 1c (29 km away) and 2c
262 (108 km away). VHF radiation in Fig. 1c remained very intense up to the end of the record, while
263 in Fig. 2c it was generally weaker and the counts and strengths of VHF sources dropped after
264 120 ms to very low values, suggesting a different discharge development. We inspected the time
265 evolution of both strength and count of raw LMA station data for the 128 events and found that
266 for three quarters of them the intense VHF radiation continued to occur at least for the closest
267 LMA station up to the end of the 208-ms long magnetic-field record, similarly to Fig. 1c. For the

268 remaining quarterof cases, the VHF radiation substantially dropped at all LMA stations before
269 the end of the magnetic-field record, similarly to Fig. 2c.

270 We illustrate the propagation of discharges starting with the isolated breakdown pulses in
271 Figs. 1d-f and 2d-f. Each dot represents one geo-located VHF source color-coded by its time of
272 occurrence. The discharge in Fig. 1 started at an altitude of about 2 km, moved up by about two
273 kilometers in 30 ms, and kept propagating with nearly horizontal branches in a limited interval of
274 altitudes for 100 ms (Fig. 1b). Finally, one branch moved down back to the initiation altitude and
275 the other one propagated horizontally. This discharge was recorded during a weak lightning
276 activity (7 discharges over 20 min). It was the first discharge of a 3-discharge sequence of 150-
277 second duration with a similar vertical distribution of geo-located VHF sources. The discharge in
278 Fig. 2 shortly propagated almost at a constant altitude (Fig. 2b). This discharge was also recorded
279 during a rather weak lightning activity (7 discharges in 12 minutes). After combining all 3D
280 propagation maps with the information about the presence/absence of VHF sources detected at
281 individual LMA stations for all isolated breakdown events, we identify two different propagation
282 scenarios: the discharges continue to propagate horizontally for more than 150 ms (Type A, as in
283 Fig. 1 – 73 %), or they fade out sooner than 150ms (Type B, as in Fig. 2 – 27 %).

284 We inspected the magnetic field waveforms of individual pulse trains in order to compare
285 their characteristics with typical signature of PB pulse trains prior -CGs: duration of about 1-2
286 ms, inter-pulse intervals of about 100 μ s, and a regular distribution of bipolar pulses (Nag and
287 Rakov, 2008). We have found that the majority of the pulse sequences lasted about two
288 milliseconds or less for both scenarios (91% of type A events:, 94% of type B events); the pulses
289 within the trains were bipolar in all cases and regularly distributed in more than one half of cases
290 (57% of type A events, 66 % of type B events). Inter-pulse intervals were typically about 100 μ s

291 long (82% of type A events, 60 % of type B events). The intervals between pulses within
292 individual trains were sometimes also shorter, about 50 μ s (9% of type A events, 20 % of type B
293 events) or longer up to 150-200 μ s (9 % of type A events, 20 % of type A events).

294 In 86 % of cases for both scenarios, the pulse peak amplitudes within the entire duration
295 of trains were monotonically increasing and then decreasing or only decreasing (examples in Fig.
296 3). In the remaining 14% of cases for both scenarios, the pulse peak amplitudes were distributed
297 randomly within the pulse sequences.

298 Fig. 3e shows that the two scenarios do not imply any clear differences in terms of spatial
299 distributions of the locations of the first geo-located VHF source in each event, time-stamped
300 close to the first recognizable isolated breakdown pulse. Fig. 3f presents the distribution of peak
301 currents reported by Météorage, always corresponding to a pulse with the largest amplitude in
302 each individual sequence. Median values of the peak current are 20 kA and 17 kA for types A
303 and B, respectively. Note that these distributions are similar in both cases, and that the currents
304 might be underestimated for both categories, as shown by Kaspar et al. (2016). The distribution
305 of initiation heights for types A and B is again similar (Fig. 3g) with median values of 3.5 km
306 and 3.8 km, respectively.

307

308

309 **5. Discussion and summary**

310 We have analyzed 128 sequences of the isolated breakdown pulses observed simultaneously
311 by a broadband receiver, a LMA network, and Météorage in West Mediterranean for two
312 periods, in 2015 and in 2018. We verified findings of Kolmasova et al. (2018) that intense VHF
313 radiation in raw LMA data coincides with the first isolated breakdown pulse in the broadband
314 magnetic-field measurements and that the most intense VHF radiation are often correlated with

315 the broadband pulses. The number of geo-located VHF sources within the 208 ms-long
316 magnetic-field records, varied from units to hundreds. There were only a few geo-located VHF
317 sources occurring simultaneously with the magnetic-field isolated breakdown pulse trains. In the
318 majority of cases (85 %), the VHF sources occurring within 1 ms around the first detectable
319 isolated breakdown pulse in each event were also the most powerful ones detected during each
320 pulse train. Their power ranged from 8 to 36 dBW (~ 6 W to 4 kW), about two orders of
321 magnitude weaker than the typical VHF power accompanying Narrow Bipolar Events as
322 reported by Bandara et al. (2020), but by two orders of magnitude stronger than the typical VHF
323 radiation detected around the initiation event of -CG flashes or normal IC discharges (Marshall et
324 al., 2019).

325 We have identified two scenarios of the isolated breakdown process based on the 128
326 sequences: the discharge continues to propagate horizontally for more than 150 ms (Type A - 73
327 %) or dies out sooner (Type B - 27 %). Typical in-cloud currents, which generated the strongest
328 isolated breakdown pulses are similar for both types. These currents are reported by Météorage
329 around 20 kA and they do not differ from peak currents, which emitted the most intense PB
330 pulses preceding -CG discharges in Florida, US (Karunarathne et al., 2019). Typical initiation
331 altitudes (3.5 km, similar for both types) correspond to the region between the main negative and
332 lower positive charge centers, where -CG discharges are initiated (Stolzenburg and Marshall,
333 2008). Geo-located VHF sources occurring close to the first detectable magnetic-field pulses in
334 both types of trains also exhibited similarly strong power (on average 24 dBW). Our analysis of
335 pulse train wave shapes shows that isolated breakdown pulse trains of both types cannot be
336 distinguished from the reported pulse sequences preceding -CG discharges (e.g., Kolmasova et
337 al., 2014, 2018, 2019; Zhang et al, 2015; Smith et al, 2018) and exhibit different properties

338 compared to the ones of initiation pulses preceding normal IC discharges (Nag and Rakov, 2008;
339 Nag et al., 2009). These results therefore indicate that isolated breakdown processes of both
340 types correspond to usual -CG discharges, which failed to propagate to ground. Several modeling
341 investigations (Nag and Rakov et al., 2009; Tan et al., 2014; and Iudin et al., 2017) show that an
342 excessive LPCR can play a crucial role in blocking the propagation of the CG discharges through
343 a potential well. Figs 1S and 2S in the Supporting Information show how this potential well
344 changes as a function of LPCR properties. Both a larger strength and/or a lower altitude of the
345 LPCR can lead to the development of a positive potential well below it. Our results are
346 consistent with the outcomes from Iudin et al. (2017) even though they used a different LPCR
347 charge distribution, position, radius, and thickness. Our results also agree with observation from
348 Coleman et al. (2008) who combined balloon measurements of vertical electric field and LMA
349 VHF sources and found that horizontal extensions of lightning channels correlated with
350 potential extrema.

351 In conclusion, we find that the isolated breakdown events (also known as attempted -CG
352 leaders, inverted IC discharges, low-level IC flashes, or PB-type flashes) can show two different
353 discharge propagation scenarios: the discharge either continues to propagate horizontally or
354 quickly fades out. Based on the observed duration of the isolated breakdown pulse trains, on the
355 inter-pulse intervals, on their regularity, and on the bipolar shapes of the pulses, as well as on the
356 geo-localization of their sources, we find that both scenarios described in this study are similar to
357 PB processes preceding -CG flashes. More studies are needed to detail the geographical or
358 seasonal variation of these two types of the isolated breakdown processes and their relation to the
359 microphysical and electrical structure of the parent thunderstorms.

360

361 **Acknowledgements**

362 The work of IK and OS was supported by European Regional Development Fund-Project
363 CRREAT (CZ.02.1.01/0.0/0.0/15_003/0000481) and by the Praemium Academiae award of the
364 Czech Academy of Sciences. The work of PK, AK, RL and LU was supported by the GACR
365 grant 20-09671S. The work from ED, SC and SP was supported by CNES through the SOLID
366 project and by ANR through the ANR-16-CE04-0005 EXAEDRE project. The SAETTA
367 network was operated with the support from CNES, HyMeX program, and Collectivité de Corse.
368 The broadband data are available at <http://bleska.ufa.cas.cz/ersa/storage/tar/>. The SAETTA data
369 are available at http://babeta.ufa.cas.cz/repository/data_2020GL090593.html.

370 **References**

- 371 Bandara, S., T. Marshall, S. Karunarathne, & M. Stolzenburg (2020), Electric field change and
372 VHF waveforms of Positive Narrow Bipolar Events in Mississippi thunderstorms, *Atmos.*
373 *Res.*243, doi:org/10.1016/j.atmosres.2020.105000.
- 374 Bazelyan, E. M., & Y. P. Raizer (2000), *Lightning physics and lightning protection*. CRC Press.
- 375 Blanc, E., F. Lefeuvre, R. Roussel-Dupré, & J. Sauvaud (2007), TARANIS: A microsatellite
376 project dedicated to the study of impulsive transfers of energy between the Earth
377 atmosphere, the ionosphere, and the magnetosphere, *Adv. Space Res.*, 40(8), 1268–1275,
378 doi:10.1016/j.asr.2007.06.037.
- 379 Chilingarian, A., Khanikyants, Y., Rakov, V. A., & Soghomonyan, S. (2020). Termination of
380 thunderstorm-related bursts of energetic radiation and particles by inverted intracloud and
381 hybrid lightning discharges. *Atmospheric Research*, 233, 104713
- 382 Coleman, L. M., M. Stolzenburg, T. C. Marshall, & M. Stanley (2008), Horizontal lightning
383 propagation, preliminary breakdown, and electric potential in New Mexico
384 thunderstorms. *J. of Geophys. Res.: Atm.*, 113(D9), doi: 10.1029/2007JD009459.
- 385 Coquillat, S., Defer, E., de Guibert, P., Lambert, D., Pinty, J.-P., Pont, V., Prieur, S., Thomas, R.
386 J., Krehbiel, P. R., and Rison, W.: SAETTA: high-resolution 3-D mapping of the total
387 lightning activity in the Mediterranean Basin over Corsica, with a focus on a mesoscale
388 convective system event, *Atmos. Meas. Tech.*, 12, 5765–5790,
389 <https://doi.org/10.5194/amt-12-5765-2019>, 2019.
- 410 Iudin, D. I., V. A. Rakov, E. A. Mareev, F. D. Iudin, A. A. Syssoev, & S. S. Davydenko (2017),
411 Advanced numerical model of lightning development: Application to studying the role of
412 LPCR in determining lightning type, *J. Geophys. Res. Atmos.*, 122, 6416–6430,
413 doi:10.1002/2016JD026261.

414 Kašpar, P., O. Santolík, I. Kolmašová, & T. Farges (2016), A model of preliminary breakdown
415 pulse peak currents and their relation to the observed electric field pulses, *Geophys. Res.
416 Lett.*, 43, doi:10.1002/2016GL071483.

417 Kolmašová, I., O. Santolík, T. Farges, W. Rison, R. Lán, & L. Uhlíř (2014), Properties of the
418 unusually short pulse sequences occurring prior to the first strokes of negative cloud-to-
419 ground lightning flashes, *Geophys. Res. Lett.*, 41, 5316–5324,
420 doi:10.1002/2014GL060913.

421 Kolmašová, I., O. Santolík, T. Farges, S. A. Cummer, R. Lán, and L. Uhlíř (2016),
422 Subionospheric propagation and peak currents of preliminary breakdown pulses before
423 negative cloud-to-ground lightning discharges, *Geophys. Res. Lett.*, 43, 1382–1391,
424 doi:10.1002/2015GL067364.

425 Kolmašová, I., O. Santolík, E. Defier, W. Rison, S. Coquillat, S. Pedebay, et al. (2018), Lightning
426 initiation: Strong VHF radiation sources accompanying preliminary breakdown pulses
427 during lightning initiation, *Scientific Reports*, volume 8, Article number: 3650,
428 doi:10.1038/s41598-018-21972-z.

429 Kotovsky, D. A., R. C. Moore, Y. Zhu, M. D. Tran, V. A. Rakov, J. T. Pilkey, et al. (2016),
430 Initial breakdown and fast leaders in lightning discharges producing long-lasting
431 disturbances of the lower ionosphere, *J. Geophys. Res. Space Physics*, 121, 5794–5804,
432 doi:10.1002/2015JA022266.

433 Ma, D. (2017), Characteristic pulse trains of preliminary breakdown in four isolated small
434 thunderstorms, *J. Geophys. Res. Atmos.*, 122, 3361–3373, doi:10.1002/2016JD025899.

435 Mansell, E. R., D. R. MacGorman, C. L. Ziegler, & J. M. Straka (2002), Simulated three-
436 dimensional branched lightning in a numerical thunderstorm model, *J. Geophys. Res.*
437 *Atmos.*, 107(D9), doi: 10.1029/2000JD000244.

438 Marshall, T., W. Schulz, N. Karunarathna, S. Karunarathne, M. Stolzenburg, C. Vergeiner, & T.
439 Warner (2014a), On the percentage of lightning flashes that begin with initial breakdown
440 pulses, *J. Geophys. Res. Atmos.*, 119, 445–460, doi:10.1002/2013JD020854.

441 Marshall, T., M. Stolzenburg, N. Karunarathna, & S. Karunarathne (2014b), Electromagnetic
442 activity before initial breakdown pulses of lightning, *J. Geophys. Res. Atmos.*, 119,
443 12,558–12,574, doi:10.1002/2014JD022155.

444 Marshall, T., S. Bandara, N. Karunarathne, S. Karunarathne, I. Kolmasova, R. Siedlecki, & M.
445 Stolzenburg (2019), A study of lightning flash initiation prior to the first initial
446 breakdown pulse, *Atmospheric Research* 217, 10-23, doi:10.1016/j.atmosres.2018.10.013.

447 Mazur, V. & L. H. Ruhnke (1998), Model of electric charges in thunderstorms and associated
448 lightning. *J. Geophys. Res. Atmos.*, 103(D18), 23299-23308, doi:0.1029/98JD02120.

449 Nag, A. & V. A. Rakov (2008), Pulse trains that are characteristic of preliminary breakdown in
450 cloud-to-ground lightning but are not followed by return stroke pulses, *J. Geophys. Res.*
451 *113*, D01102.

452 Nag, A., & V. A. Rakov (2009), Some inferences on the role of lower positive charge
453 region in facilitating different types of lightning. *Geophysical Research Letters*,
454 36(5).

455 Nag, A., B. A. DeCarlo, & V. A. Rakov (2009), Analysis of microsecond- and submicrosecond-
456 scale electric field pulses produced by cloud and ground lightning discharges,
457 *Atmospheric Research* 91, 316–325, doi:10.1016/j.atmosres.2008.01.014.

458 Pedebay, S. & M. Toullec (2016), Impact study of the ‘Millau Bridge’ on the local lightning
459 occurrence. in *International Lightning Protection Symposium 2016*.
460 Press, W. H., S. A. Teukolsky, W. T. Vetterling, & B. P. Flannery (1996), *Numerical recipes in*
461 *C*, volume 2. Citeseer.

462 Rakov, V. A., & M. A. Uman (2003), *Lightning – Physics and effects*, Cambridge University
463 Press, ISBN:9780521583275.

464 Rison, W., R.J. Thomas, P.R. Krehbiel, T. Hamlin, & J. Harlin (1999), A GPS-based Three-
465 Dimensional Lightning Mapping System: Initial Observations in Central New Mexico,
466 *Geophys. Res. Lett.*, 26, No. 23, 3573-3576.

467 Smith, E. M., Marshall, T. C., Karunarathne, S., Siedlecki, R., & Stolzenburg, M. (2018). Initial
468 breakdown pulse parameters in intracloud and cloud-to-ground lightning flashes. *J.*
469 *Geophys. Res. Atmos.* 123, 2129–2140, doi:10.1002/2017JD027729.

470 Schulz, W., G. Diendorfer, S. Pedebay, & D. Roel Poelman (2016), The European lightning
471 location system EUCLID - Part 1: Performance analysis and validation. *Nat. Hazards*
472 *Earth Syst. Sci.* **16**, 595–605.

473 Sharma, S.R., V. Cooray, & M. Fernando (2008), Isolated breakdown activity in Swedish
474 lightning, *J. Atmos. Sol.-Terr. Phys.* 70, 1213– 1221, doi:10.1016/j.jastp.2008.03.003.

475 Stolzenburg, M. & T. C. Marshall (2008), Charge structure and dynamics in thunderstorms.
476 *Space Science Reviews*, 137, 355-372, doi:10.1007/s11214-008-9338-z.

477 Tan, Y., S. Tao, & B. Zhu (2006), Fine-resolution simulation of the channel structures and
478 propagation features of intracloud lightning. *Geophys. Res. Lett.*, 33(9),
479 doi:10.1029/2005GL025523.

480 Tan, Y., S. Tao, Z. Liang, and B. Zhu (2014), Numerical study on relationship between lightning
481 types and distribution of space charge and electric potential, *J. Geophys. Res. Atmos.*,
482 109, 1003–1014, doi:10.1002/2013JD019983.

483 Thomas, R. J., P. R. Krehbiel, W. Rison, S. J. Hunyady, W. P. Winn, T. Hamlin, & J. Harlin
484 (2004), Accuracy of the Lightning Mapping Array, *J. Geophys. Res.*, 109, D14207,
485 doi:10.1029/2004JD004549.

486 Zhang, Y., Zhang, Y., Zheng, D., & Lu, W. (2015). Preliminary breakdown, following lightning
487 discharge processes and lower positive charge region. *Atmospheric Research*, 161, 52-56.

488 Zhang, Y., Krehbiel, P. R., & Liu, X. (2002). Polarity inverted intracloud discharges and electric
489 charge structure of thunderstorm. *Chinese Science Bulletin*, 47(20), 1725-1729

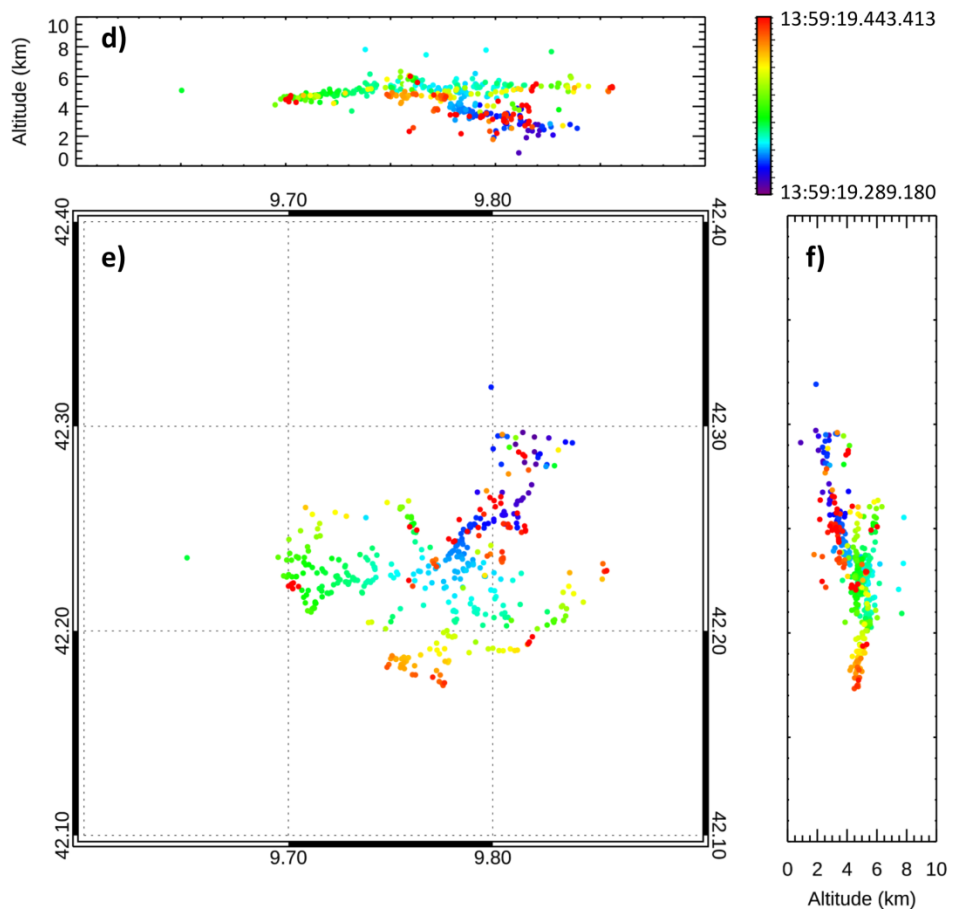
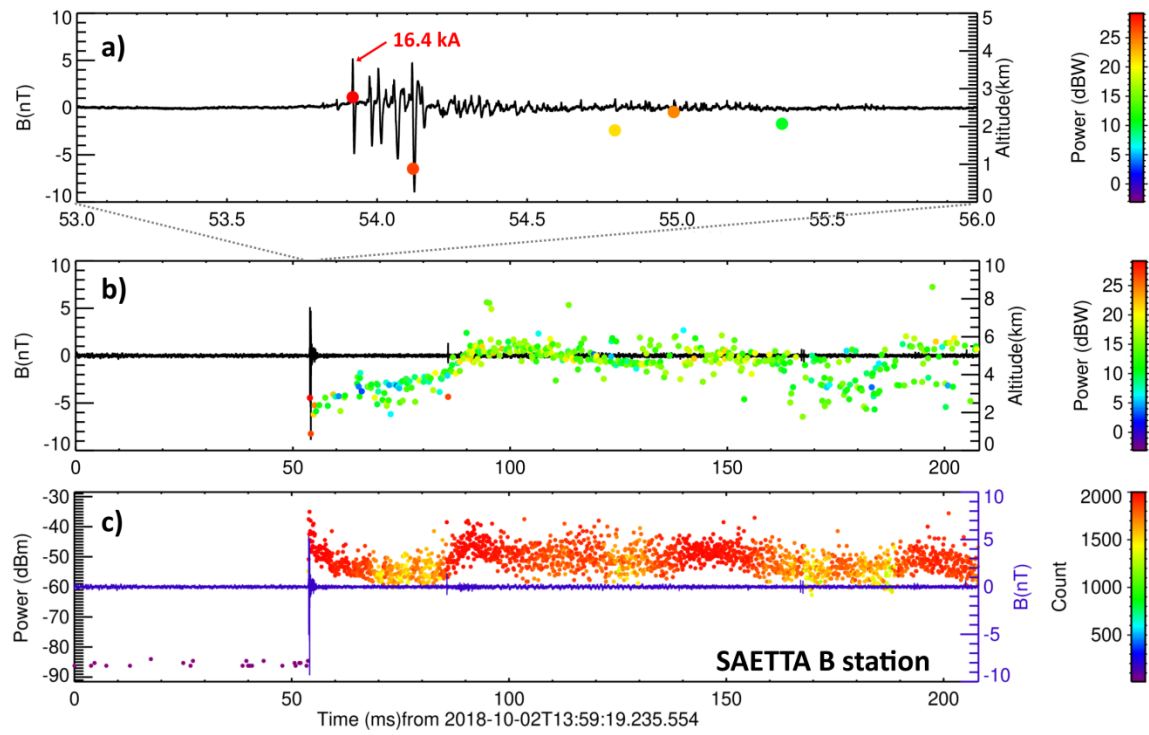
490

491

492

493

494 **Fig. 1**



496 **Fig.1** Example of an isolated breakdown event (type A) occurring on 2 Oct 2018 at 13:55:19.236
497 UT: (a) 3-ms long detail of the BLESKA waveform showing a sequence of isolated breakdown
498 pulses overlaid on altitude of geo-located SAETTA VHF radiation sources color-coded by their
499 power; (b) the whole 208 ms-long BLESKA record with geo-located VHF radiation sources; (c)
500 the BLESKA record with peaks of radiated VHF power recorded at the SAETTA station B
501 (color-coded by their counts within individual 80 μ s LMA windows); (d–f) 3D location of VHF
502 radiation sources color-coded by time (7 SAETTA stations minimum, $\chi^2 < 1$).

503

504

505

506 **Fig. 2** Same as Fig. 1 but for an isolated breakdown event (type B) occurring on 13 Oct 2015 at
507 22:09:30.073 UT.

508

509

510

511

512

513

514

515

516

517

518

519

520

521

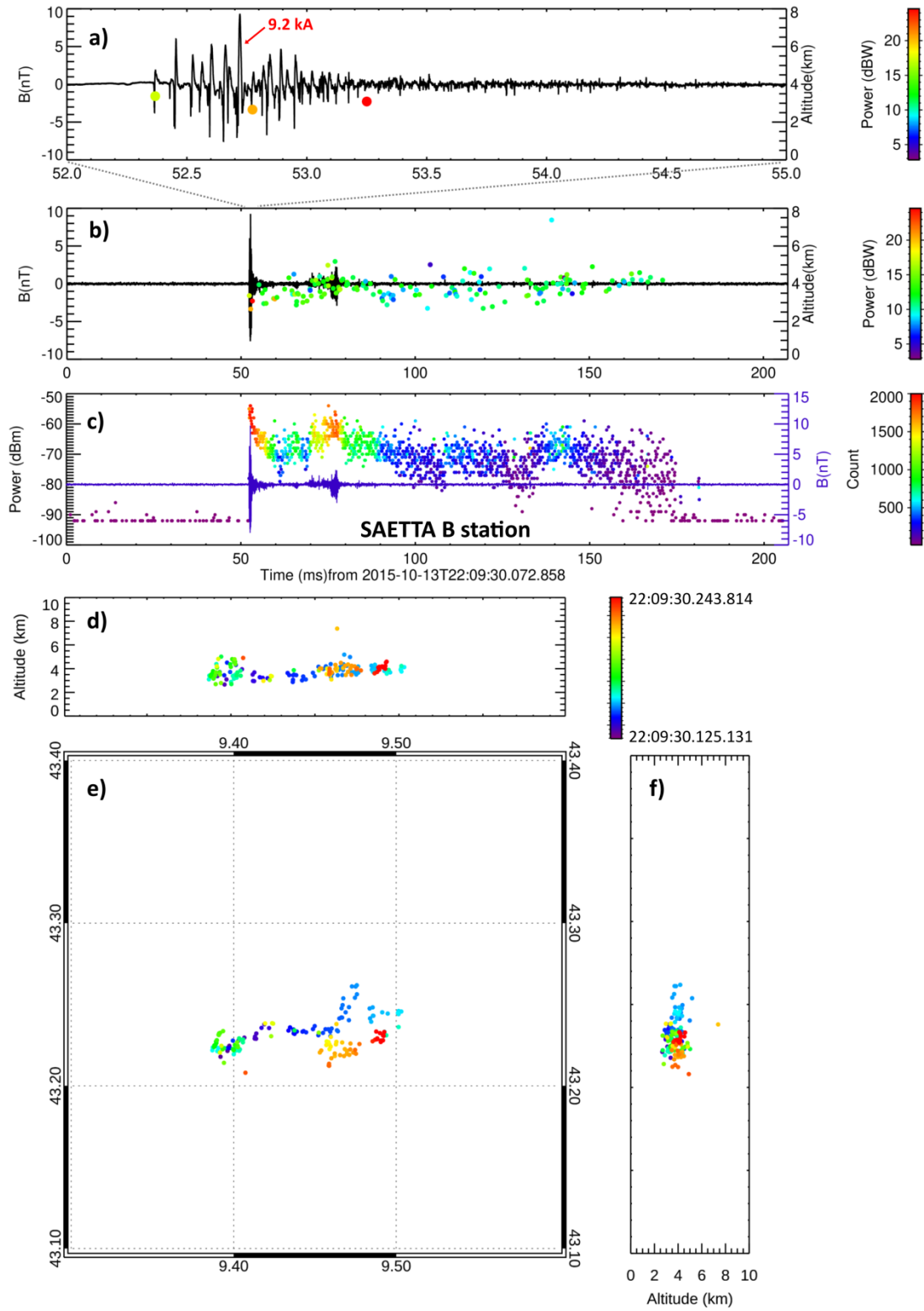
522

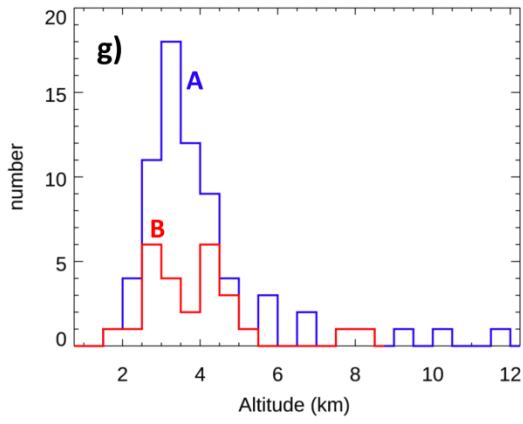
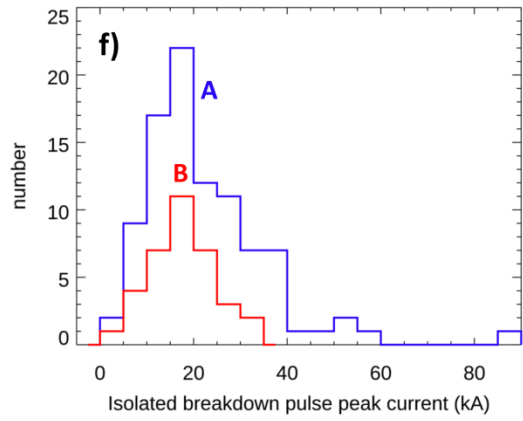
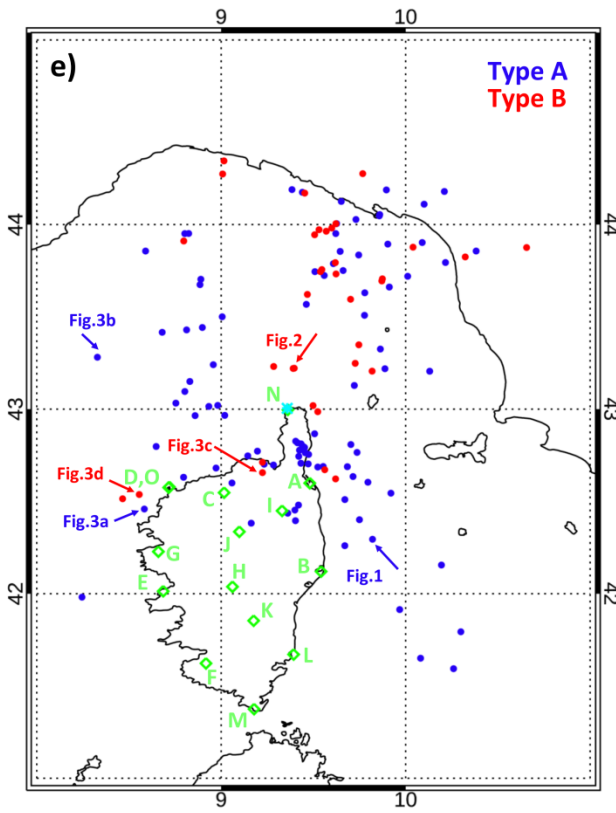
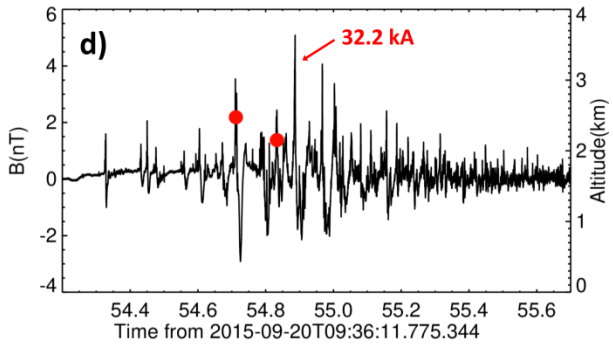
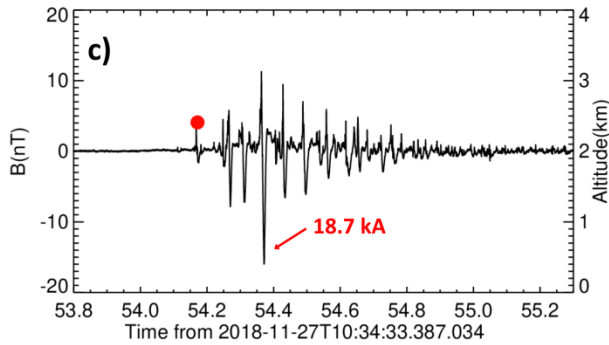
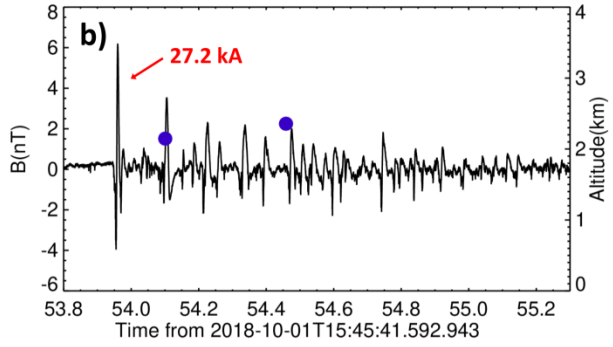
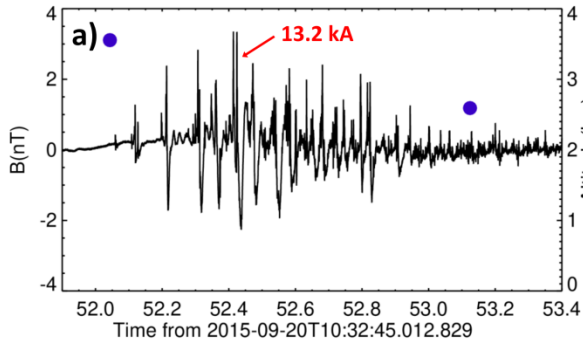
523

524

525

526 **Fig. 2**





530

531

532 **Fig.3** a-d) 1.5-ms long details of the BLESKA waveform showing sequences of isolated
533 breakdown pulses overlaid on altitude of geo-located SAETTA VHF radiation sources: (a)
534 isolated breakdown event (type A) occurring on 20 Sep 2015 at 10:32:45.013 UT, (b) isolated
535 breakdown event (type A) occurring on 01 Oct 2018 at 15:45:41.593 UT, (c) isolated breakdown
536 event (type B) occurring on 27 Nov 2018 at 10:34:33.387, (d) isolated breakdown event (type B)
537 occurring on 20 Sep 2015 at 09:36:11.775 UT, (e) Map showing the 2D location of the geo-
538 located VHF sources occurring within 1ms from the first recognizable magnetic-field pulse
539 (blue: type A, red: type B). Green diamonds show the locations of SAETTA stations. The light
540 blue star locates the BLESKA receiver. The blue and red arrows point to the events shown in
541 Figs. 1, 2, and 3a-d, respectively. (f) Histograms of the Météorage peak current corresponding to
542 largest pulses identified within magnetic-field pulse sequences; (g) Histograms of initiation
543 heights obtained as altitudes of the LMA geo-located sources occurring within 1ms from the first
544 recognizable isolated breakdown pulse (altitude uncertainty: ~20 m above Corsica and up ~500
545 m at 200 km from the coast).

546

547

548

549

550

551

552

553

554

555

556